Generation of large-scale vortex dislocations in a three-dimensional wake-type flow

LING Guocan (凌国灿) & XIONG Zhongmin (熊忠民)

State Key Laboratory of Nonlinear Mechanics, Institute of Mechanics, Chinese Academy of Sciences, Beijing 100080, China

Received January 11, 2001

Abstract Numerical study of three-dimensional evolution of wake-type flow and vortex dislocations is performed by using a compact finite diffenence-Fourier spectral method to solve 3-D incompressible Navier-Stokes equations. A local spanwise nonuniformity in momentum defect is imposed on the incoming wake-type flow. The present numerical results have shown that the flow instability leads to three-dimensional vortex streets, whose frequency, phase as well as the strength vary with the span caused by the local nonuniformity. The vortex dislocations are generated in the nonuniform region and the large-scale chain-like vortex linkage structures in the dislocations are shown. The generation and the characteristics of the vortex dislocations are described in detail.

Keywords: **vortex dislocations, nonuniform wake-type flow, DNS.**

1 Background

The wake transition behind a circular cylinder for low and moderate Reynolds numbers has receieved a great deal of attention due to its theoretical and practical significance. A comprehensive review on those researches before 1996 has been given recently by Williamson[1]. Experimental studies have shown that three-dimensional transition of the wake flow is mainly characterized by the appearance of two fundamental modes of small-scale streamwise vortices with spanwise wavelength of around 3—4 diameters and 1 diameter of the cylinder respectively for a range of Reynolds number from 180 to 260, corresponding to two discontinuities in relation of Strohaul frequency and Reynolds number. These two kinds of vortex shedding pattern, denoted by mode A and mode B respectively by Williamson, are triggered by the three-dimensional instability of the ideal two-dimensional periodic flow around the cylinder. It has been shown by examining the linear instability using low-dimensional Galerkin method[2,3] and high accurate numerical method respectively[4]. Yet there is another different instability process during the transition, called "vortex-adhesion mode"[5], when a finite disturbance to the initial flow conditions is imposed. Recently, numerical results on direct numerical simulation of wake transition from two-dimensional to three-dimensional states and to turbulence have been reported by Henderson[6], Persillon and Braza[7], Ling et al.[8], Zhang et al.[5] and Karniadakis and Triantafyllou[9], among others. Nonlinear dynamics and pattern formation as well as physical analysis of the transition are described in detail in those investigations.

In addition to those features of the transition mentioned above, Williamson[10] has further demonstrated experimentally that the wake transition also involves another fundamental phe-

nomenon, namely the appearance of large-scale spot-like vortex structures with a highly three-dimensional configuration, referred to as "vortex dislocations" by him. The vortex dislocations are generated between spanwise vortex shedding cells of different frequency, originating in the vortex formation region and growing downstream. The generation and the spatiotemporal evolution of the vortex dislocation are visualized in detail. The effect of vortex dislocations on wake velocity measurements are reported. The mechanism by which the vortex dislocations develop is discussed. It is also found that there are distinct similarities between the periodic forced "dislocations" and the intermittent "dislocations" occurring in natural transition. The experimental study suggested that the presence of these vortex dislocations can explain the large intermittent velocity irregularities in the wake to characterize the transition, which was first discovered by Roshko[11] and later by Bloor[12], and is largely responsible for the break-up to turbulence as it travels downstream. Therefore it is closely associated with a new kind of transition mechanism. The "vortex adhesion mode" proposed by Zhang et al. is characterized by spot-like vortex deformation, which is mainly induced by the spanwise non-uniformity in vortex shedding. The origin is similar to the "vortex dislocations". Actually, a number of experimental studies on three-dimensionalities of wake flows caused by spanwise nonuniformity in either cylinder diameter or incoming flows have shown that the vortex dislocations are a fundamental feature of the bluff body wakes. All of these flows are similar in behavior. In these flows Strouhal frequency varies with the span of the cylinder and the wake behavior must accommodate the rate of change of the shedding frequency along the span. Depending on flow conditions, vortex linkages across a vortex dislocation are highly three-dimensional, and present different modes. A detailed presentation of them can also be found in experimental investigations of Lewis and Gharib[13], Eisenlohr and Eckelmann[14], Gerrard[15], Gaster[16], Bearman[17], So and Maekawa[18] among others. Beside the cylinder wakes, there are a number of other kind flows exhibiting similar features of the "vortex dislocations" during their transition, such as spatially growing free shear layer[19], Taylor vortex system, Kármán vortex streets[20] and even the Rayleigh-Benard convection patterns[21].

Theoretical studies have been undertaken in an attempt to explore the dynamics of the vortex dislocations. Noack et al.[22] studied the cell formation in vortex streets by Van der Pol oscillation equation. The Ginzburg-Landau equations are also employed by Albarède and Provansal[23] in one-dimensional formulation, and by Park and Redekopp[24] in two-dimensional formulation to mimic the quasi-periodic cylinder wakes and to explain the underlying dynamic processes. Based on the Ginzburg-Landau equations and by experimental measurements Monkewitz et al.[25] modeled successfully the response of vortex shedding patterns to time-dependent boundary conditions imposed at the cylinder ends. Through the analysis of the characteristics of these model equations, some corresponding phase patterns of the vortex dislocations and their dynamics are successfully revealed and the mechanism of their formation are also discussed in terms of the analogy studies. However these model equations did not deal with the real physical flow itself.

So far, although previous studies have been concerned with the vortex dislocation problem, a large part of information comes from experiments. The understanding of the generation, the three-dimensional characteristics and the dynamics of the vortex dislocations is far from complete. No numerical study based on the Navier-Stokes equations, governing the dynamics of the flow evolution, to our knowledges, has been performed now, but it is valuable for a better understanding of the problems[1)]. Moreover, there are several unanswered questions regarding the transition

and the vortex dislocations in wake-type shear flows with local spanwise nonuniformity. For these reasons the present numerical study will address those issues. This paper will mainly focus on the generation and the characteristics of the vortex dislocations. This study tries to simplify the complex shedding phenomena induced by a real cylinder with diameter variation using a wake-type shear flow profile with local spanwise variation in streamwise velocity defect, and gain some new insights into the mechanism of vortex dislocations appearing in real flows. Following the "concept of computational reducibility"[26], it is also expected that the vortex wake will be reproduced numerically by only knowing the time-average velocity profile at specific location behind a circular cylinder where it is most unstable according to the linear instability analysis. With different time-average inlet velocity profiles obtained from previous experiments, we can get vortex streets with different shedding frequencies along the span of the flow. By studying the evolution of this kind flow, we expect to obtain the vortex dislocation phenomena and the vortex linkages and, meanwhile to save large computation resources. Direct numerical simulations of the vortex dislocations in flow passing a real circular cylinder and physical analysis are now undertaken and will be reported in a succeeding paper.

2 Compact finite difference-Fourier spectral method

Vortex dislocation structure is a kind of large scale flow structure developed in the three-dimensional open space flow, so it should be numerically investigated by the spatiotemporal mode simulation, which means that the computational domain must contain a sufficient streamwise length and the appropriate inlet and outlet boundary conditions are used to accommodate the evolution process when the large-scale vortex travels downstream. For this purpose, a compact finite difference-Fourier spectral method is employed to solve the three-dimensional incompressible Navier-Stokes equations in primitive variable formulation, which is proposed by the present authors. For details the readers may refer to refs. [27,28]. A breif introduction is as follows.

In the method the periodic boundary condition is assumed to be in the spanwise direction, and the flow variables $\boldsymbol{u} = \{u, v, w\}$, p, denoted by ϕ, are expanded into a truncated Fourier series:

$$\phi(x, y, z, t) = \sum_{m=-\frac{N}{2}}^{\frac{N}{2}-1} \phi_m(x, y, t) \cdot e^{-im\beta \cdot z}, \qquad m = -\frac{N}{2}, \cdots, \frac{N}{2} - 1, \tag{2.1}$$

where N is the cutoff, and β is the spanwise wavenumber. The three-dimensional incompressible Navier-Stokes equations in primitive variable nondimensional formulation are written as

$$\nabla \cdot \boldsymbol{u} = 0, \tag{2.2.1}$$

$$\frac{\partial \boldsymbol{u}}{\partial t} + (\boldsymbol{u} \cdot \nabla)\boldsymbol{u} = -\nabla p + \frac{1}{Re}\nabla^2 \boldsymbol{u}, \tag{2.2.2}$$

where $\boldsymbol{u} = \{u, v, w\}$ are the velocity components in x, y, z directions respectively, and p is the pressure, normalized by a characteristic free stream velocity U_0, length d, and dynamic head $\frac{1}{2}\rho_0 U_0^2$, respectively. Time t is normalized by d/U_0, and Re is the Reynolds number, defined by $U_0 d/\nu$.

1) When checking the present paper's proof, we found a recent numerical study with the title successive stages and the role of natural vortex dislocations in three-dimensional wake transition, published in Journal Fluid Mech., Vol. 439, 2001, by M. Braza et al.

From (2.1) and (2.2.2) a system of equations for the m-th Fourier component in a two-dimensional (x, y) domain are

$$\frac{\partial \boldsymbol{u}_m}{\partial t} + F_m[(\boldsymbol{u}\cdot\nabla)\boldsymbol{u}] = -\nabla_m p_m + \frac{1}{Re}\nabla_m^2 \boldsymbol{u}_m, \qquad m = -\frac{N}{2},\cdots,\frac{N}{2}-1, \tag{2.3}$$

where $\nabla_m \equiv \left\{\frac{\partial}{\partial x}, \frac{\partial}{\partial y}, -\mathrm{i}m\beta\right\}$, $\nabla_m^2 \equiv \left\{\frac{\partial^2}{\partial x^2}, \frac{\partial^2}{\partial y^2}, -m^2\beta^2\right\}$, $F_m[(\boldsymbol{u}\cdot\nabla)\boldsymbol{u}]$ is the Fourier transformation of the nonlinear terms. For time discretization to those equations a third order mixed explicit-implicit time discretization scheme[27—29] is used, the solution procedure of (2.3) can be split into the following three substeps:

$$\frac{\boldsymbol{u}'_m - \sum_{q=0}^{J_i-1}\alpha_q \boldsymbol{u}_m^{n-q}}{\Delta t} = -\sum_{q=0}^{J_e-1}\beta_q F_m[(\boldsymbol{u}^{n-q}\cdot\nabla)\boldsymbol{u}^{n-q}], \tag{2.4.1}$$

$$\frac{\boldsymbol{u}''_m - \boldsymbol{u}'_m}{\Delta t} = -\nabla_m p_m^{n+1}, \tag{2.4.2}$$

$$\frac{\gamma_0 \boldsymbol{u}_m^{n+1} - \boldsymbol{u}''_m}{\Delta t} = \frac{1}{Re}\nabla_m^2 \boldsymbol{u}_m^{n+1}, \tag{2.4.3}$$

where $\boldsymbol{u}'_m$, $\boldsymbol{u}''_m$ are intermediate velocities; J_i, J_e are parameters for the order of the scheme, and α_q, β_q, γ_0 are appropriately chosen weights. For the third order case, the values of these coefficients are summarized as follows[29]:

$$J_e = 3,\ J_i = 3,\ \alpha_0 = 3,\ \alpha_1 = -\frac{3}{2},\ \alpha_2 = \frac{1}{3},\ \beta_0 = 3,\ \beta_1 = -3,\ \beta_2 = 1,\ \gamma_0 = \frac{11}{6}.$$

To evaluate the nonlinear term $F_m[(\boldsymbol{u}^{n-q}\cdot\nabla)\boldsymbol{u}^{n-q}]$ on the right-hand side of (2.4.1), the pseudo-spectral method is adopted. When the Fourier coefficients of velocities are transformed into the velocities in the physical space, the nonlinear convection terms are approximated by the fifth-order upwind compact schemes[27,28].

By (2.4.2) and (2.4.3), following Helmholtz equations for the pressure (derived after taking the divergence of (2.4.2)) and velocities must be solved in each step to obtain p_m^{n+1} and $\boldsymbol{u}_m^{n+1}$:

$$\frac{\partial^2 \phi}{\partial x^2} + \frac{\partial^2 \phi}{\partial y^2} - b\phi = f. \tag{2.5}$$

f includes the derivations of the Fourier coefficients $\boldsymbol{u}_m$ in the x and y directions. They are approximated by the sixth-order center compact schemes[30].

In order to match the high accuracy of the explicit approximation of the $F_m[(\boldsymbol{u}^{n-q}\cdot\nabla)\boldsymbol{u}^{n-q}]$ and f, and meet the requirements of numerical stability and convergence, (2.5) should be discretized by high order implicit scheme, too. Therefore, the following nine-point compact scheme of the fourth-order accuracy is derived[27,28]:

$$\frac{10(\phi_1+\phi_3) - 2(\phi_2+\phi_4) + (\phi_5+\phi_6+\phi_7+\phi_8) - 20\phi_0}{(\Delta x)^2}$$
$$+ \frac{10(\phi_2+\phi_4) - 2(\phi_1+\phi_3) + (\phi_5+\phi_6+\phi_7+\phi_8) - 20\phi_0}{(\Delta y)^2}$$

$$-(8\phi_0+\phi_1+\phi_2+\phi_3+\phi_4)b=(8f_0+f_1+f_2+f_3+f_4).$$

This hybrid method provides not only high numerical accuracy and wavenumber resolution but also the flexible capability to treat the complex boundary conditions.

The inflow velocity profile is taken as

$$U(y,z)=1.0-a(z)(2.0-\cosh(by)^2)e^{-(cy)^2}, \tag{2.6}$$

which represents the time average streamwise velocity profile in the cylinder near wake. The parameters $a=1.1+0.4e^{-z^2}$, $b=1.1$, $c=1.2$, are determined by direct numerical simulations[9] as well as the experimental measurements[31]. The profile flow of $U(y,z)$ will be shown numerically to be absolute unstable. The introduction of $a(z)$ represents the three-dimensional disturbance to the two-dimensional cylinder wake. At the center of the span, $z=0$, the velocity defect is the maximum. Away from the center the rate of the defect decays exponentially to zero, where the free stream behaves two-dimensionally. The velocity profile (2.1) mimics the existence of a local non-uniformity in the cylinder diameter along the span, e.g. with a ring whose diameter is slightly larger than the cylinder's diameter. Fig. 1 shows the inflow velocity profiles at $z=0$ and $z=16$.

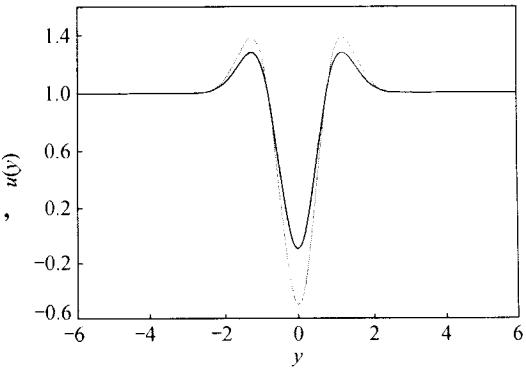

Fig. 1. Velocity profile of wake-type incoming flow. ——, At the spanwise boundaries ($z=\pm 16$); ……, at the spanwise center ($z=0$).

For the pressure boundary conditions, with formulas (2.3) and (2.4), the semi-discretized representation can be written as

$$\frac{\partial p_m^{n+1}}{\partial n}=\boldsymbol{n}\cdot\left\{-\frac{\partial \boldsymbol{u}_m}{\partial t}+\frac{1}{Re}\nabla^2\boldsymbol{u}_m^{n+1}-\sum_{q=0}^{J_e-1}\beta_q F_m[(\boldsymbol{u}^{n-q}\cdot\nabla)\boldsymbol{u}^{n-q}]\right\}$$

$$=\boldsymbol{n}\cdot\left\{-\frac{\partial \boldsymbol{u}_m}{\partial t}-\frac{1}{Re}F_m[\nabla\times\Omega^n]-\sum_{q=0}^{J_e-1}\beta_q F_m[(\boldsymbol{u}^{n-q}\cdot\nabla)\boldsymbol{u}^{n-q}]\right\}, \tag{2.7}$$

where $\nabla^2\boldsymbol{u}\equiv\nabla D-\nabla\times\Omega$, $\Omega\equiv\nabla\times\boldsymbol{u}$, $D\equiv\nabla\cdot\boldsymbol{u}$. By forcing $D^{n+1}\equiv 0$ in each time step and replacing $\nabla\times\Omega^{n+1}$ by $\nabla\times\Omega^n$, the divergence-free constraint can be well satisfied on the boundaries.

For a finite computing domain, correctly setting the outflow boundary conditions in the incompressible flow, generally speaking, is quite insufficient. It is hoped that the outflow boundary conditions can closely approximate the free space situation which exists in the absence of these boundaries. Otherwise, the spurious perturbation waves may propagate upstream and severely affect the accuracy of computation in the inner flow domain. Recently, Jin et al.[32] developed a new kind of nonreflecting-type outflow boundary conditions on the analogy of the classical wave equation. It deals with both the nonlinear and diffusive mechanism of flow and well matches the Navier-Stoke equations adopted inside the domain. By preliminary computations, we found that the performance of this kind of boundary conditions is quite suitable to the numerical simulation of external flows, especially those involving the interaction between waves and vortices. Generalized to the three-dimensional case, the nonreflecting boundary condition in physical space can be formulated as

$$\frac{\partial \boldsymbol{u}}{\partial t} + \boldsymbol{u}\frac{\partial \boldsymbol{u}}{\partial x} = \frac{1}{Re}\left(\frac{\partial^2 \boldsymbol{u}}{\partial y^2} + \frac{\partial^2 \boldsymbol{u}}{\partial z^2}\right). \tag{2.8}$$

We noticed that a similar result was also obtained in ref. [33] recently. The corresponding spectral form used in the computation is

$$\frac{\partial \boldsymbol{u}_m}{\partial t} + F_m\left[u\frac{\partial \boldsymbol{u}}{\partial x}\right] = \frac{1}{Re}\left(\frac{\partial^2 \boldsymbol{u}_m}{\partial y^2} - m^2\beta^2 \boldsymbol{u}_m\right). \tag{2.9}$$

Eq. (2.9) must be solved simultaneously with the same third order mixed explicit-implicit schemes adopted for Navier-Stokes equations in the inner domain.

In the present computation, Reynolds number is taken as 200. The computational domains are 60, 30, 30 in streamwise, vertical and spanwise directions, respectively. The cutoff of the truncated Fourier series is $N = 32$, and the corresponding grid points in x-y plane is 122×62.

3 Numerical results

In this paragraph we will first show the general characteristics of the wake-type flow evolution and the three-dimensionalities of the flow caused by the local spanwise nonuniformity in incoming flow. Then we describe in detail the vortex dislocations and the large-scale chain-like vortex structures generated downstream in a narrow spanwise region around the center.

The present results have demonstrated numerically the instability of the three-dimensional incoming wake-type flow. Fig. 2 gives the instantaneous distributions of the spanwise vorticity at different spanwise locations at $t = 89.74$. It shows the spatial evolution of the wake-type flow: upstream, the onset of the instability waves, a little downstream, the rolling-up of the vortices and further downstream, the formation of Kármán vortex streets. Notice that the wavelengths of the vortex street at the position $z = 16$ are approximately five times that of the characteristic length d, in agreement with common experimental results. However, at $z = 0$ in streamwise direction the vortex street seems to become one row of vortices. The ratio of the width to wave length is much less than that at the boundaries. This distinct sectional flow pattern implies that there has been a specific three-dimensional vortex structure across the center of the span. Moreover, the two vortex streets are not generated at the same time nor take place at the same streamwise locations, showing that there is a phase difference between them.

Spectral analysis for time series of velocity component $v(t)$ at $z = 0$ and $z = 16$ yields two independent frequencies $f_c = 0.1346$ and $f_b = 0.1538$, respectively, corresponding to two vortex streets produced by the global instability of the inflow velocity profiles as shown in fig. 2(a) and 2(b). The vortex shedding frequency in the central part of the span is lower than at the boundary, which is different from common experimental results. In experiments reported by Gerich and Eckelmann[33], at the ends of the cylinder, as they are located in boundary layer, the cells have a lower shedding frequency than in the central part of the span. However, in the present calculation, there is no such a kind of end effect. The interaction between f_c and f_b is also shown by the appearance of the peak at $f_c + f_b$.

Fig. 3 shows the profiles of the fluctuating streamwise velocities u_{rms} at different streamwise locations, with $z = 0$ at the center (a) and $z = 16$ at the boundary (b). Near the center region of the vertical direction (y) there is a darkened area where the maximum gradient of u_{rms} appears, the vortex street begins to shape. Again, we can see that the rapid growth of the fluctuating energy in upstream designates the onset of the nonlinear development of the flow instability, leading to

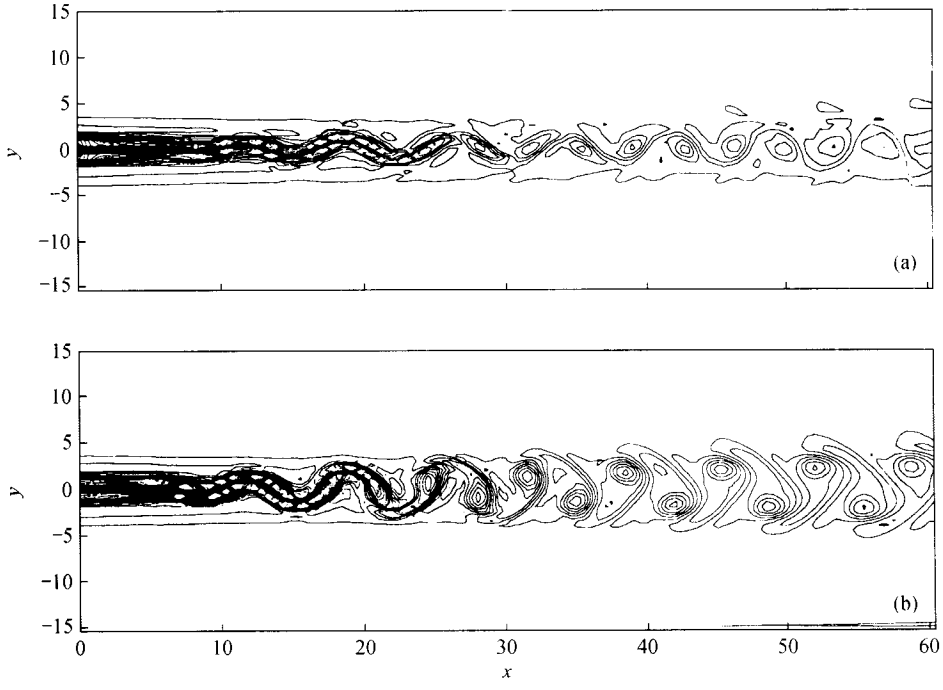

Fig. 2. Spanwise vorticity contour on x-y plane at $z = 0$ (a) and $z = 16$ (b).

a Kármán vortex street. These distinct fluctuaction energy distributions further show the existense of a specific vortex structure in the center area of the span.

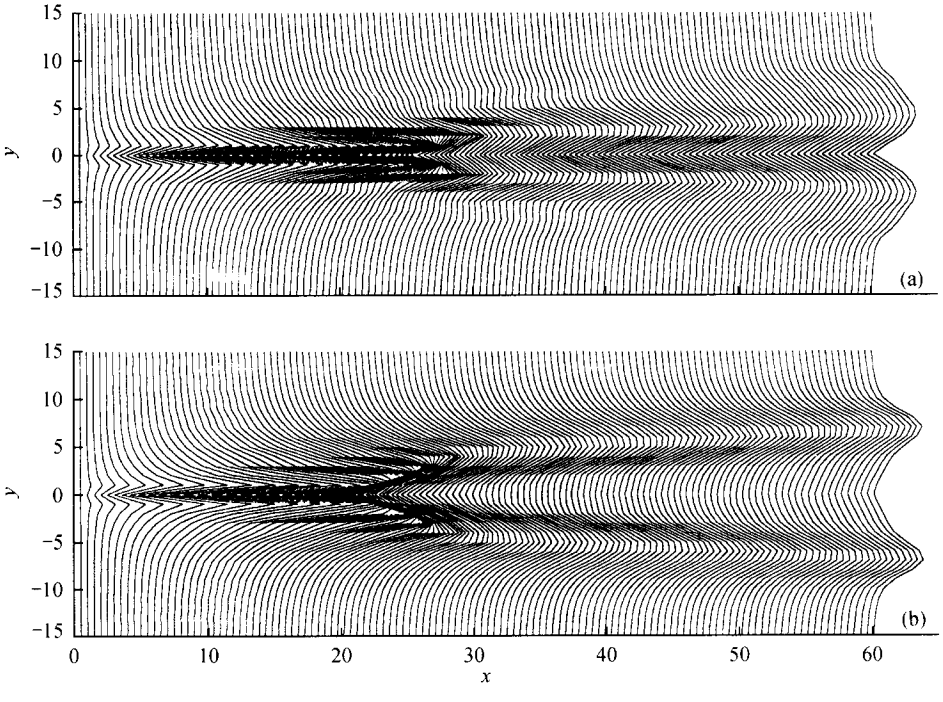

Fig. 3. The profiles of fluctuating velocity u_{rms} on different x-y planes, $z = 0$ (a) and $z = 16$ (b).

From the above numerical results, it is clear that the temporal and spatial evolution of the incoming flow leads to a three-dimensional vortex flow field. The local nonuniformity causes the differences between vortex streets in frequency and phase along the span, especially in vortex strength, which we will discuss later, in a narrow region around the center. Thus, the vortex dislocations between the adjecent vortex streets occur. The wake flow has to accommodate these changes between vortex streets at their interface. A symmetric vortex dislocation pattern is expected to be produced.

The spanwise vorticity contours in x-z plane at $y = 0$ and $y = 1$ are shown in fig. 4. In this top view picture, the spanwise vortices with positive sign and negative sign are arranged consecutively in the streamwise direction. In the center region of the span the former are twisted and connected with the latter, indicating that the streamwise vorticity structures are generated and develop into certain kinds of "bridge" between the spanwise vortices. However, out of the center region, the spanwise vortices appear like two-dimensional vortex tubes.

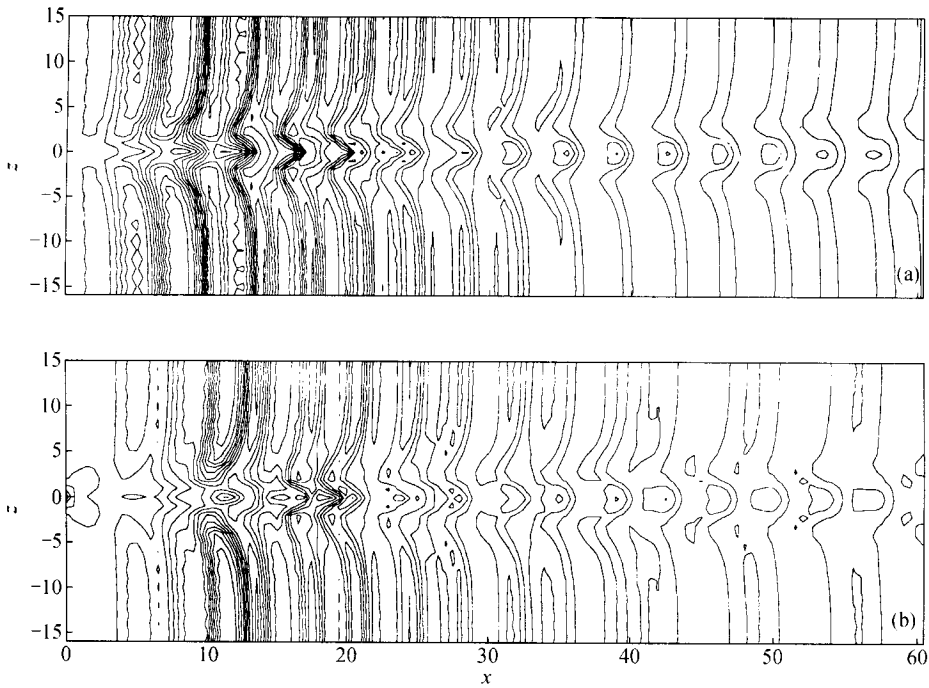

Fig. 4. Spanwise vorticity contours on x-z plane at $y = 0$ (a) and $y = 1$ (b) respectively.

For details of the global characteristics of the three-dimensional flow field, some data visualization is also generated. Fig. 5 shows the isosurface of the three-dimensional vorticity field. It exhibits two distinct regions: out of the center part of the span, the appearance of the vortices are very like a two-dimensional vortex roll, but, in the center part of the span, a large-scale chain-like three-dimensional vortex structure with complex configuration occurs. It can be seen that the structure appears periodic streamwise with a wavelength of the base flow and symmetric in the spanwise direction. Clearly, the topological change in vortices involves the large distortion to streamwise direction and splitting of the original spanwise vortices, the split vortex bending to form streamwise vortex loops and connecting with spanwise vortices. In the figure, it is clear that the vortex connection between the spanwise vortices takes place by cross-vortex street mode; that

is, the split small vortex connects with its neighbouring spanwise vortex that follows and is on the other side of the vortex street with an opposite sign.

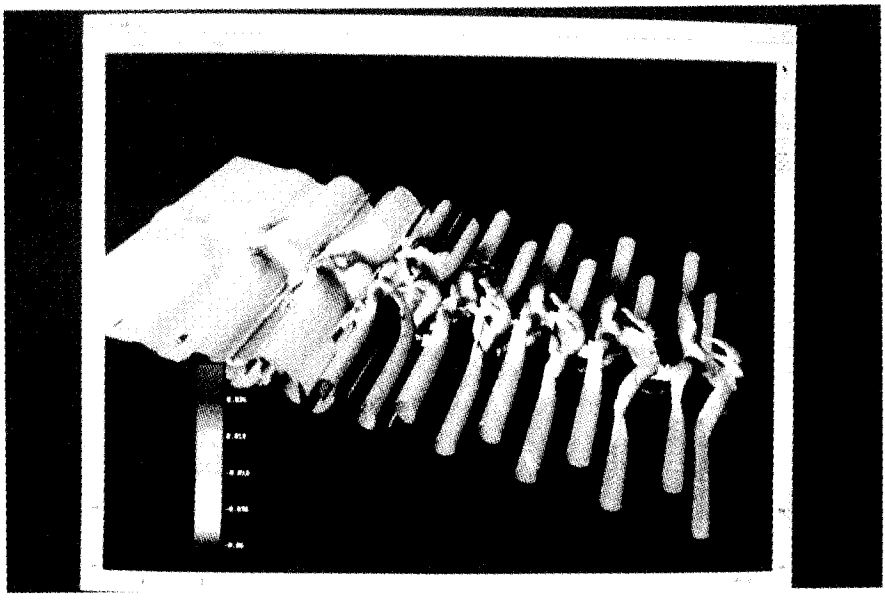

Fig. 5

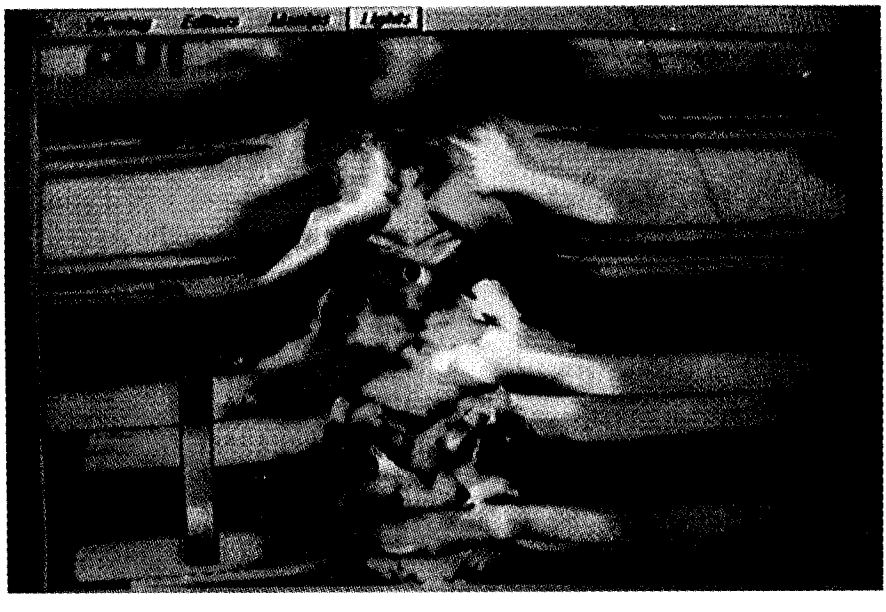

Fig. 6

Fig. 6 is a top view of a close-up of the vortex splitting process during the formation of the vortex dislocations. In the figure the flow is downwards. It can be thought again that the spanwise velocities are generated from the complex vortex tearing and in turn lead to lateral spreading of the vortex structure from the center.

An explanation for formation of the large-scale chain-like vortex structures can be proposed

based on vortex dynamics. Due to the phase and frequency difference between the adjecent vortex streets, the transition of the spanwise vortex in the center region of the span will be crossed by an inclined path. Besides, from the wake type flow (2.6) it can be estimated that the circulation of each vortex in a sectional vortex street will vary with the span. It decreases rapidly from a maximum to a lower constant value across the center of the span. For circulation conservation, the surplus circulation at the interface must be split out and bent to streamwise direction by the induction velocity of the spanwise vortex. Again, due to the induction function, the streamwise vortex loops, consisting of the split vortex lines, appear up on a spanwise vortex with positive sign, and then occur under another successive spanwise vortex with negative sign. The aspect of the large-scale vortex structure, therefore, looks wavy and chain-shaped. Comparing the present results with those in cylinder wakes caused by spanwise variation in either diameter or velocity, we see that there are some basic similarities in behavior, namely the vortex line continuity and the original vortex lines parallel to spanwise axis, more or less, bending to streamwise direction, which was first pointed out by Gerrard and later further confirmed by Lewis and Gharib and Williamson in their experiments. Now these basic features are shown in detail by the present numerical study in the wake-type flow. However, in the present case, the vortex flow are triggered by the instability, the vortex dislocations are generated in nonlinear waves (Kármán vortices), and the specific characteristics of vortex dislocations and the dynamic process are rather different from those in cylinder wakes.

Beside the vortex splitting, the present computed results show that the secondary flows in the axial direction of the spanwise vortex are also induced in the process of vortex dislocations (not shown here). The large velocity magnitude occurs at the locations corresponding to the spanwise vortex core region. These results are the same as those induced by the vortex dislocations in cylinder wake, as reported by ref. [10]. The induced spanwise velocity, closely linked to the topological changes of the vortex structures, leads to spanwise extension of the vortex dislocations.

4 Concluding remarks

In the present study the vortex dislocations and the large-scale chain-like vortex linkages in the dislocations in wake-type flow with local spanwise nonuniformity have been shown, for the first time, by the direct numerical simulation. Numerical results have demonstrated the instability of the incoming flow which leads to a three-dimensional vortex street field. The local nonuniformity imposed in a narrow spanwise region of the wake-type flow causes differences between the vortex streets in phase, frequency and strength. The large-scale chain-like vortex dislocations across the center of the span are generated. They appear periodic in the streamwise direction and symmetric about the center of the span. The characteristics of the large-scale vortex linkages such as large distortion and splitting of original spanwise vortex, bending of the split vortex lines as well as the streamwise vortex loops are described in detail. The dynamical mechanism for the formation is suggested.

The purpose of the present paper is to show numerically the generation and the basic features of the vortex dislocations in a typical wake type flow. Obviously a wealth of numerical study and theoretical analysis work are yet to be done in this field. These remain the topics for further research.

Acknowledgments This work was supported by the Special Founds for Major State Basic Research Projects (G1999032801), and by the National Climbing A Pre-selected Projects and the National Natural Science Foundation of China. Computational resources

were provided by NCFC computer center, CAS. The helpful suggestions from Refereé are acknowledged.

References

1. Williamson, C. H. K., Vortex dynamics in the cylinder wake, Annu. Rev. of Fluid Mech., 1996, 28: 477—539.
2. Noack, B. R., Eckelmann, H., A global stability analysis of the steady and periodic cylinder wake, J. Fluid Mech., 1994, 270: 297.
3. Ling Guocan, Chang Yong, Three-dimensional stability analysis of the periodic wake behind a circular cylinder by low-dimensional Galerkin method, Acta Mechanica Sinica (in Chinese), 1999, 31: 660.
4. Barkley, D., Henderson, R. D., Three-dimensional Floquet stability analysis of the wake of a circular cylinder, J. Fluid Mech., 1996, 322: 215.
5. Zhang, H. Q., Fey, U., Noack, B. R. et al., On the transition of cylinder wake, Phys. Fluids, 1995, A7(4): 779.
6. Henderson, R. D., Nonlinear dynamics and pattern formation in turbulent wake transition, J. Fluid Mech., 1997, 352: 65.
7. Persillon, H., Braza, M., Physical analysis of the transition to turbulence in the wake of a circular cylinder by three-dimensional Navier-Stokes simulation, J. Fluid Mech., 1998, 365: 23.
8. Ling Guocan, Yu Chenwei, Xiong Zhongmin, The nonlinear features of the wake transition behind a circular cylinder, Proceedings of the Third China-Japan Workshop on Turbulent Flows, Beijing, China, 31 Oct.—4 Nov., 1998.
9. Karniadakis, G. E., Triantafyllou, G. S., Three-dimensional dynamics and transition to turbulence in the wake of bluff objects, J. Fluid Mech., 1992, 238: 1.
10. Williamson, C. H. K., The natural and forced formation of spot-like 'vortex dislocations' in the transition of a wake, J. Fluid Mech., 1992, 243: 393.
11. Roshko, A., On the development of turbulent wakes from vortex streets, NACA Rep., 1954, 119.
12. Bloor, M. S., The transition to turbulence in the wake of a circular cylinder, J. Fluid Mech., 1964, 19: 290.
13. Lewis, C., Gharib, M., An exploration of the wake three-dimensionalities caused by a local discontinuity in cylinder diameter, Phys. Fluids, 1992, A4: 104.
14. Eisenlohr, H., Eckelmann, H., Vortex splitting and its consequences in the vortex street wake of cylinders at low Reynolds number, Phys. Fluids, 1989, 1: 189.
15. Gerrard, J. H., The three-dimensional structure of the wake of a circular cylinder, J. Fluid Mech., 1996, 25: 143.
16. Gaster, M., Vortex shedding from circular cylinder at low Reynolds number, J. Fluid Mech., 1971, 46: 749.
17. Bearman, P. W., Challenging problems in bluff body wakes, bluff-body wakes, dynamics and instabilities, IUTAM Symposium Göttingen/Germany, 1992, 19.
18. So, A., Maekawa, H., Study of vortex dislocations in the wake of a flat plate with finite thickness, Transactions of the Japan Society of Mechanical Engineers B, 2000, 66: 649.
19. Browand, F. K., Troutt, T. R., The turbulent mixing layer: geometry of large vortices, J. Fluid Mech., 1985, 158: 489.
20. Ling Guocan, Xiong Zhongmin, The three dimensional flow features of interaction between two vortex streets, in Proceedings of the Eighth International Offshore and Polar Engineering Conference, Montréal, Canada, May 24—29, 1998.
21. Pocheau, A., Croquette, V., Gal, P. L., Turbulence in a cylindrical container of Argon near threshold of convection, Phys. Rev. Lett., 1985, 55: 1094.
22. Noack, B. R., Ohle, F., Eckelmann, H., On the cell formation in vortex streets, J. Fluid Mech., 1991, 227: 293.
23. Albarède, R., Provansal, M., Quasi-periodic cylinder wakes and the Ginzburg-Landau model. J. Fluid Mech., 1995, 291: 191.
24. Park, D. S., Redekopp, L. G., Selection principles for spatio-temporal patterns in wake flows, in Proc. IUTAM Symp. on Bluff-body Wake, Dynamics, and Instability, Göttingen, Sept. 7—11, 1992.
25. Monkewitz, P. A., Williamson, C. H. K., Miller, G. D., Phase dynamics of Kármán vortices in cylinder wakes, Phys. Fluids, A, 1996, 8: 91.
26. Triantafyllou, G. S., Karniadakis, G. E., Computational reducibility of unsteady viscous flows, Phys. Fluids A, 1990, 2: 653.
27. Xiong, Z. M., Ling, G. C., Compact finite difference-Fourier spectral method for three dimensional incompressible Navier-Stokes equation, Acta Mechanica Sinica, 1996, 12(4): 296.
28. Xiong, Z. M., Ling, G. C., Compact finite difference-Fourier spectral method for the three dimensional incompressible Navier-Stokes equations and application to vortex dislocation, Plenary Lecture, Fifteenth International Conference on Numerical Methods in Fluid Dynamics, June 24—28, 1996, Monterey, CA, USA, Lecture Notes in Physics, LNP, 490.
29. Kaniadakis, G. E., Israeli, S. A., Orzag, S. A., High-order splitting methods for the incompressible Navier-Stokes equations, J. Comput. Phys., 1994, 97: 414.
30. Lele, S. K., Compact finite difference schemes with spectral-like resolution, J. Comput. Phys., 1992, 103: 16.
31. Nishioka, M., Sato, H., Measurements of velocity distributions in the wake of a circular cylinder at low Reynolds numbers, J. Fluid Mech., 1974, 65: 97.
32. Jin, G., Braza, M., A nonreflecting outlet boundary condition for incompressible unsteady Navier-Stokes calculation, J. Comput Phys., 1993, 107: 239.
33. Gerich, D., Eckelmann, H., Influence of end plates and free ends on the shedding frequency of circular cylinders, J. Fluids Mech., 1982, 122: 109.